Evaluation of diffusion mechanisms in NiAl by embedded-atom and first-principles calculations

Y. Mishin
School of Computational Sciences, George Mason University, Fairfax, Virginia 22030

A. Y. Lozovoi
Atomistic Simulation Group, School of Mathematics and Physics, The Queen's University of Belfast, Belfast BT7 1NN, Northern Ireland, United Kingdom

A. Alavi
Department of Chemistry, University of Cambridge, Lensfield Road, Cambridge CB2 1EW, United Kingdom
(Received 6 July 2002; published 16 January 2003)

The energetics of Ni vacancy jumps in the intermetallic compound NiAl are studied by combining embedded-atom and first-principles calculations. The embedded-atom potential used in this work is fit to both experimental and first-principles data and provides an accurate description of point defect energies and vacancy jump barriers in NiAl. Some of the embedded-atom results reported here, are independently verified by plane-wave pseudopotential calculations. The results suggest that the atomic configuration produced by a nearest-neighbor jump of a Ni vacancy is mechanically unstable. Because of this instability, the vacancy implements two sequential nearest-neighbor jumps as one collective, two-atom transition. Such collective jumps initiate and complete six-jump vacancy cycles of a Ni vacancy, which are shown to occur by either four or three vacancy jumps. Next-nearest-neighbor vacancy jumps are shown to have diffusion rates comparable to experimental ones at the stoichiometric composition, suggesting that this is an important diffusion mechanism in NiAl.

DOI: 10.1103/PhysRevB.67.014201 PACS number(s): 61.50.Ah, 61.72.Bb, 61.72.Ji, 61.72.Nn

I. INTRODUCTION

The intermetallic compound NiAl has an ordered $B2$ (CsCl prototype) structure up to its melting point and a homogeneity range extending a few atomic percent on either side of the stoichiometry.[1] This compound demonstrates an unusual mechanism of nonstoichiometry, which is presumably shared by CoAl and CoGa and is referred to as the ''triple-defect mechanism.'' Namely, while the excess of Ni atoms in Ni-rich compositions is accommodated by the Al sublattice in the form of antisites, the excess of Al atoms in Al-rich compositions is accommodated through the formation of structural vacancies on the Ni sublattice.[2] This asymmetry in the nature of structural defects can be expected to lead to different diffusion mechanisms on either side of the stoichiometry and a combination of such mechanisms at the stoichiometry. The idea of the multiplicity of diffusion mechanisms in NiAl was supported by the early experimental work of Hancock and McDonnell,[3] who observed a nonmonotonic, V-shape concentration dependence of ^{63}Ni diffusion in NiAl with a sharp minimum at the stoichiometric composition. More recently, ^{63}Ni diffusion in NiAl was remeasured more accurately using single-crystalline samples and more sensitive detection methods.[4] Although general agreement with the previous work[3] was found, some of the effects reported by Hancock and McDonnell were not reproduced. In particular, the steep Al-rich branch of the V-curve leveled out resulting in almost identical diffusivities in Al-rich and near-stoichiometric compositions with an abrupt increase in Ni-rich compositions (>53 at. % Ni). Despite this disagreement, both sets of experimental data reveal a nonmonotonic behavior of diffusion as a function of the composition across the stoichiometry and point to a possible change in the diffusion mechanism.

On the theoretical side, although NiAl has been studied extensively over the recent years, diffusion mechanisms in this compound are not well understood. Several candidate mechanisms have been proposed, including sublattice self-diffusion by next-nearest-neighbor (NNN) vacancy jumps,[5,6] six-jump vacancy cycles (6JC's),[7–9] the antistructural bridge (ASB) mechanism,[10] and the triple-defect mechanism.[4,11] Some of the mechanisms have been evaluated by atomistic computer simulations with controversial results. For Ni diffusion, the lowest activation energy (2.76 eV in stoichiometric NiAl) was found for the NNN vacancy mechanism with slightly higher activation energies for the ASB and 6JC mechanisms.[6,12] An important property of the NNN vacancy mechanism is that it should lead to a very high Ni diffusivity in Al-rich compositions dominated by Ni vacancies. This prediction has not been supported by the experimental work of Frank *et al.*[4] From this contradiction between theory and experiment, Frank *et al.*[4] concluded that the NNN vacancy mechanism does not dominate Ni diffusion in NiAl. They have suggested[4] that the NNN vacancy mechanism is ineffective in the temperature interval of experimental measurements because of a too low attempt frequency of NNN vacancy jumps. Instead, the triple-defect mechanism has been proposed[4] to dominate Ni diffusion in NiAl. The estimated activation energy of that mechanism (3.18 eV regardless of the composition) compares reasonably well with the experimental activation energy in Al-rich and near-stoichiometric compositions (3.00 ± 0.07 eV), but fails to explain the drop in the experimental activation energy in Ni-rich compositions (>53 at. % Ni). This drop has been attributed to a contribu-

tion of the ASB mechanism arising when the concentration of antisites on the Ni sublattice reaches the respective percolation threshold.[4]

It should be pointed out that the calculated activation energies of different diffusion mechanisms are close to one another within ± 0.2 eV,[4,9] which is probably comparable to the accuracy of those calculations. The estimates of the frequency factors are even less accurate, not to mention the possible role of jump correlations and other factors that often defy accurate calculations.[13] Given these uncertainties, caution should be used when selecting the most favorable mechanism and rejecting less favorable ones. In particular, previous estimates of the role of the NNN vacancy mechanism should be taken with a grain of salt. The low attempt frequency reported in Ref. 4 (0.26 THz) was obtained with an embedded-atom method (EAM) potential[14] that had not been fit to reproduce reliable phonon frequencies. In addition, the attempt frequencies reported in Refs. 4 and 9 were based on the extrapolation scheme of the embedded-cluster method,[15–18] a procedure which has recently been recognized to be inadequate.[19,20] The same EAM potential and essentially the same calculation methods were employed for the evaluation of all other mechanisms.[4,9] There are open questions regarding the 6JC mechanism too. Gumbsch[21] suggested that the configuration arising after the first jump of a 6JC can be mechanically unstable, with the consequence that the first two and therefore the last two jumps of a cycle can happen by a collective displacement of two atoms. This means that 6JC's can be implemented in four or three vacancy jumps instead of six. This possibility calls for a careful evaluation since the number of jumps in a 6JC strongly affects the diffusion kinetics through the jump correlation factor.[8,22]

A new EAM potential has recently been constructed for NiAl by fitting to an expanded database containing both experimental properties and a large set of first-principles data generated by the full-potential linearized augmented plane-wave method in conjunction with the local-density approximation.[23] The potential provides an accurate description of basic properties of NiAl and is well transferable to a wide range of atomic configurations encountered in atomistic simulations. In particular, the potential accurately reproduces elastic properties of NiAl, phonon frequencies, thermal expansion, formation energies of point defects and planar faults, energies of several existing and computer-generated structures of the NiAl system, and energies along continuous deformation paths between such structures. The point defect energies calculated with the potential are in a better agreement with first-principles calculations than energies obtained with previous potentials. This potential and other methodological improvements of the recent years can now be applied to reexamine diffusion mechanisms in NiAl and shed more light on their relative importance.

The present paper makes the first step in that direction by reexamining the energetics of the NNN jump and 6JC mechanisms of Ni diffusion in NiAl. Along with calculations based on the EAM potential,[23] the key results are independently verified by first-principles calculations. In Sec. II, we introduce our calculation procedures and demonstrate how the EAM potential compares with first-principles calculations for point defect energies. In Sec.III, we compute the energy barriers, attempt frequencies, and rate constants for three types of Ni vacancy jump: (i) NNN jump on the Ni sublattice, (ii) jumps initiating 6JC's, which indeed turn out to be collective jumps involving two atoms, and (iii) a collective [111] vacancy jump producing two antisites. The impact of the collective nature of nearest-neighbor (NN) vacancy jumps for the 6JC mechanism are analyzed. For the NNN vacancy mechanism, the Arrhenius parameters of Ni self-diffusion in stoichiometric NiAl are calculated and compared with experimental data. In Sec. IV, we summarize our results and draw conclusions.

II. CALCULATION METHODS

A. Atomic interactions in NiAl

The EAM model[24] describes the total energy of an ensemble of atoms as a sum of two energy terms: (i) the sum of pair interactions between all atoms in the system, plus (ii) the sum of their embedding energies. The embedding energy is a function of the local electron density induced on a given atom by all other atoms. Because the pair interaction potential and the electron density are radial (angular-independent) functions, the EAM model works best for simple and noble metals, is less accurate for transition metals, and is almost inapplicable to covalent crystals. The EAM model is known to be quite adequate for NiAl.[23,25] Several EAM-type potentials have been constructed for NiAl by different groups, see an overview and references in Ref. 23. As indicated in Sec. I, the potential of Ref. 23 is the most suitable for the purpose of this work.

The first-principles calculations reported below were performed by the plane-wave pseudopotential method within the local-density approximation as implemented in the CPMD code.[26] The Ni and Al atoms were represented by norm-conserving Troullier-Martins non-local pseudopotentials.[27] The plane-wave cutoff was chosen to be 80 Ry. For $B2$-NiAl, the potential predicts the lattice parameter of 2.897 Å, the bulk modulus of 169 GPa, and the formation energy of -0.69 eV/atom. These values are in good agreement with experimental data.[28–30] For point defect calculations, a 48-atom hexagonal supercell was constructed, with the hexagonal axis parallel to the [111] direction of the $B2$-NiAl lattice. The integration over the Brillouin zone was based on 11 **k**-points within its 1/12 irreducible part.[31]

B. Point defect calculations

NiAl supports four types of point defect: vacancy on the Ni sublattice (V_{Ni}), vacancy on the Al sublattice (V_{Al}), antisite on the Ni sublattice (Al_{Ni}), and antisite on the Al sublattice (Ni_{Al}). The point defect formation energies at 0 K were calculated by static relaxation. In the EAM calculations, an $8\times8\times8$ (1024 atoms) simulation block with periodic boundary conditions was typically used, but the most important results were checked for convergence by additional calculations on smaller and larger blocks. A single-point defect was created in the center of the block and the

total energy was minimized with respect to local atomic displacements with a simultaneous volume relaxation. The ''raw energy''[13,14] of the defect was obtained as the total energy of the relaxed block with the defect minus the total energy of the initial perfect-lattice block.

Similarly, in first-principles calculations a defect was created in the 48-atom supercell and its total energy was minimized with respect to atomic positions until the Hellmann-Feynman forces on all atoms reduced to below 0.05 eV/Å. Such calculations were repeated for about ten different supercell volumes and the overall energy minimum was determined by a polynomial interpolation of the obtained energy-volume relation.[31]

The formation entropies of the point defects were calculated with the EAM potential within the classical harmonic approximation. The frequencies of normal atomic vibrations were computed by diagonalizing the dynamical matrix of the simulation block. In order to eliminate three translational degrees of freedom of the system, one corner atom of the block was fixed, while all other atoms remained dynamic. The ''raw'' formation entropy of a defect[13] was determined as the entropy of the relaxed defected block minus the entropy of the initial perfect-lattice block

$$S = k_{\mathrm{B}} \sum_{i=1}^{3N-3} \ln\frac{h\nu_i^0}{k_B T} - k_{\mathrm{B}} \sum_{i=1}^{3N_d-3} \ln\frac{h\nu_i}{k_{\mathrm{B}} T} + 3k_{\mathrm{B}}(N_d - N). \quad (1)$$

Here, N is the number of atoms in the perfect-lattice block, N_d is the number of atoms in the defected block, h is the Planck constant, k_{B} is the Boltzmann constant, T is the reference temperature, and ν_i^0 and ν_i are normal vibrational frequencies before and after the creation of the defect. The choice of T in this expression is arbitrary and does not affect any observable properties of point defects.[13] For a vacancy $N_d = N-1$, while for an antisite $N_d = N$.

C. Calculation of vacancy jump rates

Vacancy jumps rates were calculated with the EAM potential within the harmonic transition state theory.[32] In the transition state theory, the rate constant Γ (jump probability per unit time) is given by the expression

$$\Gamma = \nu_0 \exp\left(-\frac{E_m}{k_{\mathrm{B}} T}\right), \quad (2)$$

where E_m is the jump barrier (saddle-point energy minus the energy before the jump), ν_0 is the attempt frequency, and T is temperature. The attempt frequency is expressed through normal vibration frequencies of the simulation block at the saddle point (ν_i^*) and before the jump (ν_i)

$$\nu_0 = \frac{\prod_{i=1}^{3N-3} \nu_i}{\prod_{i=1}^{3N-4} \nu_i^*}. \quad (3)$$

The denominator in this expression contains one frequency less than the numerator because one eigenvalue of the dynamical matrix of the saddle-point configuration is negative. This ''missing'' vibrational degree of freedom converts to a translational degree of freedom associated with the system motion along the reaction path.

The central problem of jump rate calculations is finding the saddle point of a jump.[33] For a vacancy jump in a monoatomic crystal, the saddle point can often be found from symmetry considerations. In contrast, some of the diffusion mechanisms anticipated in ordered compounds include sequences of several vacancy jumps and may involve other point defects residing next to the jumping vacancy. Under such conditions the minimum-energy path of a vacancy jump may not have a symmetry allowing us to locate the saddle point.

Previous diffusion calculations for NiAl employed the ''drag'' method in which the atom exchanging with a vacancy was moved between its two equilibrium positions by small steps and the simulation block was partially relaxed after each step. This method has proved to be adequate in many applications, but it has the drawback that only single-atom jumps can be simulated. More advanced methods of saddle-point finding have recently been reviewed in Ref. 33. In the present work, we used the nudged-elastic band (NEB) method which had been successful for simulating a variety of rate processes in solids.[33,34] To implement the NEB method, the initial and final states of the jumps must be specified. The method starts by generating a number of copies, or ''images,'' of the system which initially represent some intermediate configurations between the initial and final states. For example, the images can be created by a linear interpolation of atomic coordinates. This set of images is referred to as an ''elastic band.'' The energy of the elastic band is defined as the sum of actual potential energies of all images plus the sum of fictitious elastic deformation energies of imaginary springs connecting neighboring images. This energy is minimized with respect to atomic displacements in all images. Some of the components of atomic and spring forces are slightly modified during the minimization process in order to improve the convergence. It can be shown that, regardless of details of the relaxation procedure, the relaxed elastic band positions itself along the minimum-energy path and thus approximates the reaction path the jump.[33,34] The image with the highest potential energy can be identified as the saddle-point, or otherwise interpolation of atomic coordinates between the highest-energy image and its neighbors on either side can be applied to locate the saddle-point more precisely. Importantly, there is no restriction on the number of atoms involved in the jump, which makes the method suitable for collective jumps involving two or more atoms.

In this work, the NEB calculations were performed on a 1024-atom block under a constant block volume corresponding to the initial state of the vacancy. The elastic band included between 25 and 30 images. Usually much less images are used in NEB calculations. In some cases as little as five-seven images were enough for obtaining credible results.[45] We chose to use much more images in order to make sure that our calculations do not miss any hidden minima along

the transition path. The energy difference between the saddle-point configuration and the initial state gave us the jump barrier E_m.

The attempt frequency calculation is a more delicate subject. Because the saddle-point structure is slightly more open than the initial state and the total volume is fixed, the saddle-point structure obtained by the NEB method is generally under some compression. The effect of this small compression on the energy barrier in a large simulation block is negligibly small, but the effect on the vibrational entropy at the saddle-point can be more significant.[20] The relevant entropy change ΔS can be estimated from the thermodynamic relation[35]

$$\left(\frac{\partial S}{\partial P}\right)_T = -\beta V, \tag{4}$$

which gives

$$\Delta S \approx -\beta P V. \tag{5}$$

Here, $\beta = V^{-1}(\partial V/\partial T)_P$ is the volume thermal-expansion factor, P is the hydrostatic pressure in the simulation block containing the saddle-point configuration, and V is the block volume.[20] The product PV can be readily calculated within the EAM scheme.[20] The thermal-expansion factor β was calculated separately by applying Eq. (5) to a 1024-atom perfect-lattice block. The vibrational entropy S was computed for a large set of pressures P and the ratio $\Delta S/PV$ was extrapolated to $P \to 0$ to give $\beta = 4.589 \times 10^{-5}\ \mathrm{K}^{-1}$. This value of β was used in conjunction with Eq. (5) for calculating the entropy correction $\exp(-\Delta S/k_B)$ to the attempt frequency due to the residual compression P at the saddle-point. In order to recover the true value of ν_0, Eq. (3) was modified as follows:

$$\nu_0 = \frac{\prod_{i=1}^{3N-3} \nu_i}{\prod_{i=1}^{3N-4} \nu_i^*} \exp\left(\frac{\beta P V}{k_B}\right). \tag{6}$$

D. Point defect complexes

Point defects should appear in NiAl in such concentrations that to preserve its chemical composition. This requirement is met automatically if we assume that point defects are generated and eliminated not each individually but in the form of composition-conserving complexes. Point defects can even be thought of as existing in the form of such complexes. It should be emphasized, however, that the defects are grouped into complexes conceptually and not physically. The complexes are assumed to be totally dissociated and interactions between their constituents are neglected. The concept of composition-conserving defect complexes has been very fruitful in analyzing atomic disorder, thermodynamic properties, and diffusion in NiAl.[36,37] In particular, thermodynamically equilibrium defect concentrations in NiAl can be expressed in terms of energies and entropies of composition-conserving complexes, which in turn can be expressed through raw energies and entropies of individual defects. All arbitrarily chosen reference values involved in raw quantities cancel out in such expressions and do not affect the complex properties. This makes the complex energies and entropies a useful base for comparing results obtained by different calculation methods.

TABLE I. Expressions for energies of composition-conserving point defect complexes in NiAl in terms of "raw" energies ε_i of individual point defects. E_0 is the cohesive energy per atom in the perfect lattice. Defect complexes: DV—divacancy; Ex—exchange defect; TN—triple-defect on the Ni sublattice; TA—triple-defect on the Al sublattice.

Complex	Expression
DV	$E_{DV} = \varepsilon_{V_{Ni}} + \varepsilon_{V_{Al}} + 2E_0$
Ex	$E_{Ex} = \varepsilon_{Ni_{Al}} + \varepsilon_{Al_{Ni}}$
TN	$E_{TN} = 2\varepsilon_{V_{Ni}} + \varepsilon_{Ni_{Al}} + 2E_0$
TA	$E_{TA} = 2\varepsilon_{V_{Al}} + \varepsilon_{Al_{Ni}} + 2E_0$

Table I gives the relevant expressions for four most commonly discussed defect complexes:[36,37] divacancy DV ($V_{Ni} + V_{Al}$), exchange defect Ex ($Al_{Ni} + Ni_{Al}$), triple-defect on the Ni sublattice TN ($2V_{Ni} + Ni_{Al}$), and triple-defect on the Al sublattice TA ($2V_{Al} + Al_{Ni}$). Similar expressions hold for complex entropies, except that the cohesive energy E_0 should be replaced by the perfect-lattice entropy per atom.

The results of first-principles calculations of complex energies are summarized in Table II. We note that the numbers obtained in this work are identical to those preliminary reported in Ref. 31. Note the significant scatter of first-principles energies obtained by different groups using slightly different methods. The EAM energies calculated for the same supercell sizes are also included in Table II for

TABLE II. Calculated formation energies (in eV) of composition-conserving point defect complexes in NiAl. N is the number of atoms in the simulation cell. Defect complexes: DV—divacancy; Ex—exchange defect; TN—triple-defect on the Ni sublattice; TA—triple defect on the Al sublattice.

Method	N	Defect complex				Reference
		DV	Ex	TN	TA	
MB-PP [a]	32	3.07	3.15	2.83	6.46	44
MB-PP [a]	16	2.98	3.32	2.85	6.43	37
	54	2.71	3.10	2.22	6.30	
LSGF [b]	54	2.53	3.63	2.36	6.32	36
PW-PP [c]	16	2.40	2.93	2.03	5.70	31
	48	2.19	2.67	1.59	5.44	
EAM [d]	16	2.540	2.975	2.456	5.600	present work
	32	2.421	2.806	2.321	5.327	
	48	2.407	2.791	2.299	5.307	
	54	2.413	2.739	2.304	5.261	

[a]Mixed-basis pseudopotential method.
[b]Locally self-consistent Green's-function method.
[c]Plane-wave pseudopotential method.
[d]Embedded-atom method.

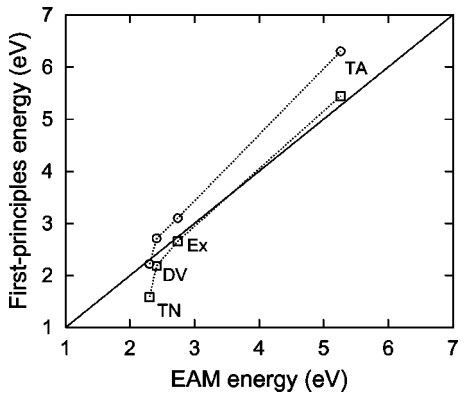

FIG. 1. Formation energies of composition-conserving point defect complexes in NiAl calculated by the EAM ($N=54$) and first-principles methods (○ – Ref. 37, $N=54$; □ – Ref. 31, $N=48$). In all calculations the complex energy increases in the same order: TN-DV-Ex-TA. The line of perfect agreement between EAM and first-principles calculations is shown as a guide to the eye.

comparison. The comparison shows that the EAM energies agree well with first-principles calculations within the scatter of the latter, indicating that the EAM potential used in this work captures the point defect energetics in NiAl quite well.

This assertion is further illustrated by plotting two most recent sets of pseudopotential energies against the respective EAM energies in Fig. 1. All data points are observed to group around the perfect agreement line. Furthermore, all three data sets follow the same ordering of the complex energies, with the energy increasing in the row TN-DV-Ex-TA. The latter agreement is important as it is the relative ranking of the energies of defect complexes that determines the type of structural[38,39] and dominant thermal[36,39] point defects in NiAl alloys. We note also that the EAM-predicted TN energy compares reasonably well with the experimental value 1.90 eV.[40]

Atomic disorder in stoichiometric NiAl is strongly dominated by triple defects TN, i.e., defect complexes $2V_{Ni}+Ni_{Al}$ consisting of two Ni vacancies and one Ni antisite. Assuming that all Ni vacancies present in the compound are associated with such triple defects, the statistical-mechanical analysis based on noninteracting defects gives the following expression for the equilibrium vacancy concentration on the Ni sublattice:[36,37]

TABLE III. Formation energies (in eV) and entropies (in k_B units) of composition-conserving point defect complexes in NiAl calculated with the EAM potential on a 1024-atom supercell. (Ref. 23) Defect complexes: DV—divacancy; Ex—exchange defect; TN—triple-defect on the Ni sublattice; TA—triple defect on the Al sublattice.

	Defect complex			
	DV	Ex	TN	TA
Energy	2.396	2.765	2.281	5.276
Entropy	2.965	4.903	3.588	7.245

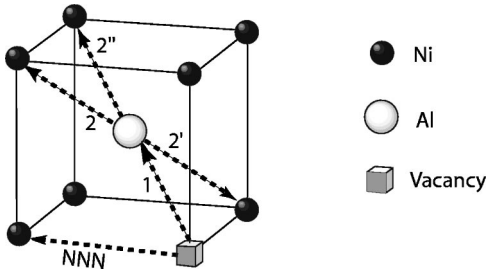

FIG. 2. Geometry of Ni vacancy jumps analyzed in this work. NNN—next-nearest-neighbor vacancy jump; 1-2, 1-2′, and 1-2″—collective vacancy jumps by vectors [110], [100], and [111], respectively.

$$c_{Ni}^{v}=2^{1/3}\exp\left(-\frac{E_{TN}-TS_{TN}}{3k_BT}\right). \quad (7)$$

Here, E_{TN} and S_{TN} are the energy and entropy of triple-defects, respectively (Table I). Similar expressions can be derived for equilibrium concentrations of other point defects.[36,37] Table III summarizes the defect complex energies and entropies required for such calculations. Equation (7) is sufficient for the purpose of this work since our analysis is focused on Ni vacancies in stoichiometric NiAl.

III. RESULTS AND DISCUSSION

A. NNN vacancy jump

Under the NNN vacancy mechanism a Ni vacancy is wandering along the Ni sublattice by exchanges with NNN Ni atoms. This mechanism is equivalent to a normal vacancy mechanism on the simple cubic lattice formed by Ni atoms (Fig. 2). The energy barrier and attempt frequency of NNN vacancy jumps have been calculated within the transition state theory and the results are reported in Table IV. The energy barrier was also calculated by the pseudopotential method, which gave $E_m=2.48$ eV in good agreement with the EAM value $E_m=2.33$ eV. To create the saddle-point configuration, a neighboring Ni atom was moved towards the vacant site by the vector (1/2)[100] dictated by the crystal symmetry. In EAM calculations, this position of the saddle-point was independently verified by the NEB method (Fig. 3). It should be pointed out that, since the first-principles calculation was performed in a relatively small block (48 atoms) under a constant volume, the obtained energy barrier should be viewed as an upper estimate of E_m. Applying the volume relaxation or/and increasing the supercell size would presumably yield a smaller value of E_m and improve the

TABLE IV. Calculated energy barrier E_m and attempt frequency ν_0 of Ni vacancy jumps in NiAl.

Jump	E_m (eV)	ν_0 (THz)
NNN	2.332	45.1
[100] collective	2.978	145.2
[110] collective	2.463	242.7
[111] collective	2.192	23.0

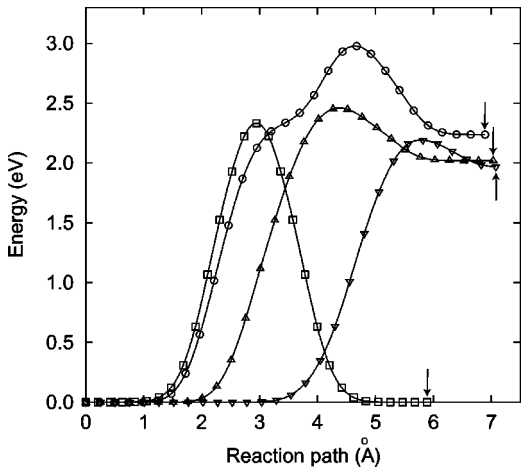

FIG. 3. Energy along the reaction path for four jumps of a Ni vacancy in NiAl. □—NNN jump; ○—collective jump initiating a [100] six-jump cycle; △—collective jump initiating a [110] six-jump cycle; ▽—collective jump by vector [111]. The energy maxima correspond to saddle-points. The arrows mark final positions of the jumps. The curves were calculated by the NEB method.

agreement with the EAM result even more. However, already this agreement dismisses the possible argument against the NNN vacancy mechanism based on the well-known trend of EAM potentials to underestimate jump barriers. The agreement with the first-principles calculation indicates that the potential used in this work provides an adequate description of saddle-point energies of vacancy jumps.

For a further evaluation of the NNN vacancy mechanism, the Ni self-diffusion coefficient D^*_{Ni} has been calculated by assuming that only this mechanism is operative. We use the standard expression[41]

$$D^*_{\mathrm{Ni}} = a^2 f_0 c^v_{\mathrm{Ni}} \Gamma, \tag{8}$$

where $f_0 = 0.653$ is the tracer self-diffusion correlation factor on a simple cubic lattice. Combining Eq. (8) with previous Eqs. (2) and (7), we obtain the Arrhenius relation

$$D^*_{\mathrm{Ni}} = D_0 \exp\left(-\frac{Q}{k_{\mathrm{B}}T}\right) \tag{9}$$

with the activation energy

$$Q = \frac{E_{\mathrm{TN}}}{3} + E_m \tag{10}$$

and the preexponential factor

$$D_0 = 2^{1/3} a^2 f_0 \nu_0 \exp\left(\frac{S_{\mathrm{TN}}}{3k_{\mathrm{B}}}\right). \tag{11}$$

Using the data from Table III, Eqs. (10) and (11) give $Q = 3.09$ eV and $D_0 = 1.6 \times 10^{-6}$ m^2/s. These numbers compare reasonably well with the experimental values $Q = 3.0$ eV and $D_0 = 3 \times 10^{-5}$m^2/s.[4] The calculated preexponential factor is on the lower side of the experimental value, but we should keep in mind that the calculation is based on the harmonic approximation which may not work well in the high-temperature range 1050–1630 K of experimental measurements, not to mention possible experimental errors. This comparison is not claimed to be a proof that Ni diffusion in stoichiometric NiAl is totally dominated by NNN vacancy jumps. At this point we can only conclude that such jumps are capable of contributing to Ni diffusion significantly and that there is no ground for rejecting them as one of possible diffusion mechanisms.

B. Collective vacancy jumps

An NN jump of a Ni vacancy creates an Al vacancy and an $\mathrm{Al_{Ni}}$ antisite as nearest neighbors. An important fact established in this work is that this configuration is *mechanically unstable*. Namely, the Al atom exchanged with the vacancy returns to its initial position during the relaxation process and we end up where we started–with a Ni vacancy. It was checked that this instability does not depend on the size of the simulation block. Furthermore, this instability was also confirmed in this work using the Ludwig and Gumbsch[42] EAM potential.

It was important to verify that the mechanical instability of the $\mathrm{V_{Al}} + \mathrm{Al_{Ni}}$ configuration is a true effect is not an artifact of EAM potentials. This fact was confirmed by first-principles calculations in a 48-atom supercell. An Al atom neighboring on a Ni vacancy was moved by a vector (1/2)[111] to fill the vacant Ni site and the obtained configuration was subject to static relaxation. Figure 4 clearly demonstrates that during the relaxation process the Al atom moves back until it fills the Al site and leaves us with a Ni vacancy. The scatter of the points in the plots is due to the use of a quasi-Newton procedure (Broyden-Fletcher-Goldfarb-Shano method[43]) for the optimization of the atomic positions: after making a small first displacement according to the current forces, the algorithm tries to guess the next, larger displacement such that to bring atomic forces down to zero, and so on until the Hessian matrix has to be reset in order to avoid an instability. Despite this scatter, we observe that the Al atom keeps moving back toward the Al vacancy until it fills it and the system arrives at equilibrium. The system energy also decreases monotonically as a function of the number of iterations and does not show any signs of a jump barrier, which proves that the $\mathrm{V_{Al}} + \mathrm{Al_{Ni}}$ configuration is truly unstable.

As a consequence of this instability, we can expect that a Ni vacancy will move by making two sequential NN jumps as one collective, two-atom displacement. Figure 2 demonstrates that there are three geometrically possible collective jumps of a Ni vacancy. The jumps 1-2 and 1-2′ have a special significance since they initiate [110] and [100] 6JC's, respectively.[8,6] The 1-2″ jump by vector [111] is not associated with any known diffusion mechanism but may presumably operate as a mechanism of antisite defect generation. Each of these jumps produces two additional antisites, so that the respective defect reaction can be written as

$$\mathrm{V_{Ni}} \rightarrow \mathrm{V_{Ni}} + \mathrm{Ni_{Al}} + \mathrm{Al_{Ni}}. \tag{12}$$

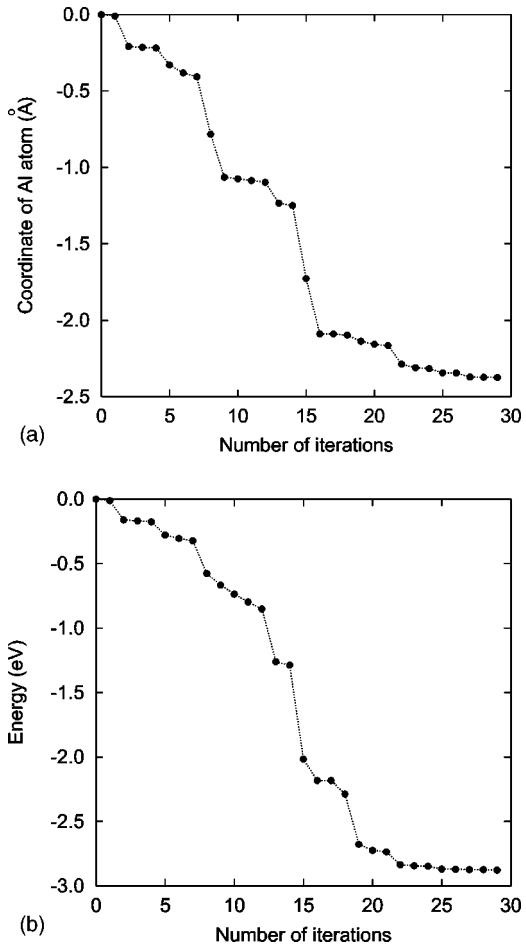

FIG. 4. Distance along the [111] direction (a) and the total energy (b) relative to the initial position of the Al atom in the $V_{Al} + Al_{Ni}$ configuration as a function of the number of iterations performed during the static relaxation process. The calculations were performed by the pseudopotential method on a 48-atom supercell. The monotonic decrease in the distance and energy indicates that the initial configuration is mechanically unstable and transforms to a Ni vacancy during the relaxation process.

The energy along the reaction paths of the collective vacancy jumps calculated by the NEB method is plotted in Fig. 3. The distance along the path is Euclidean distance between neighboring images in the $3N$-dimensional configuration space of the system, N being the number of atoms. The points on each path represent individual images of the elastic band. The occurrence of only one energy maximum on each path proves that the two NN jumps happen as a collective two-atom process and not as two separate single-atom jumps. For the [100] and [110] jumps, this means that the first two jumps of a 6JC occur as one collective jump. By symmetry, the last two jumps of a cycle should also occur as one collective jump.

Furthermore, by analogy we could expect that the two medium NN jumps of a 6JC would also merge into one collective jump. In the case of a [110] 6JC this turns out to be true. By calculating the reaction path of the two medium NN jumps by the NEB method we have found that the jumps indeed happen as one collective, two-atom transition. In other words, the central configuration of a [110] 6JC, $V_{Al} + 2Al_{Ni} + Ni_{Al}$, delivers a maximum of the total energy and not a minimum, meaning that this configuration is mechanically unstable. The energy along the overall reaction path of a [110] 6JC is plotted in Fig. 5(a). This plot demonstrates that the cycle consists of *three atomic transitions* as it was suggested by Gumbsch,[21] and not six single-atom jumps as it was thought before. We note that a three-jump mechanism was also discussed for 6JCs of Al vacancies in FeAl.[22] In contrast, for both the straight and bent [100] cycles the central configuration is mechanically stable and these cycles are implemented by four vacancy jumps [Figs. 5(b,c)].

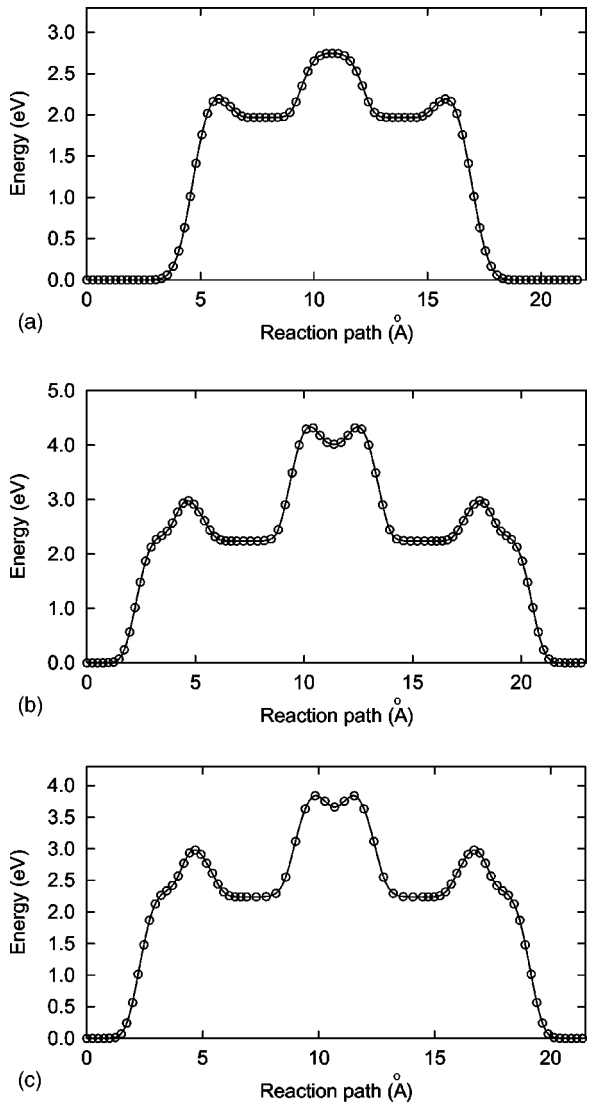

FIG. 5. Energy along the reaction path for a [110] six-jump cycle (a), straight [100] six-jump cycle (b), and bent [100] six-jump cycle (c) of a Ni vacancy in NiAl. See Refs. 8 and 6 for geometric details of 6JCs in the B2 structure. The energy maxima correspond to saddle-points, the energy minima to stable configurations. The curves were calculated by the NEB method with the embedded-atom potential of Ref. 23. The curve shapes around energy minima and maxima may depend on the choice of the stiffness constant of the imaginary springs, but the energies themselves do not depend on that choice.

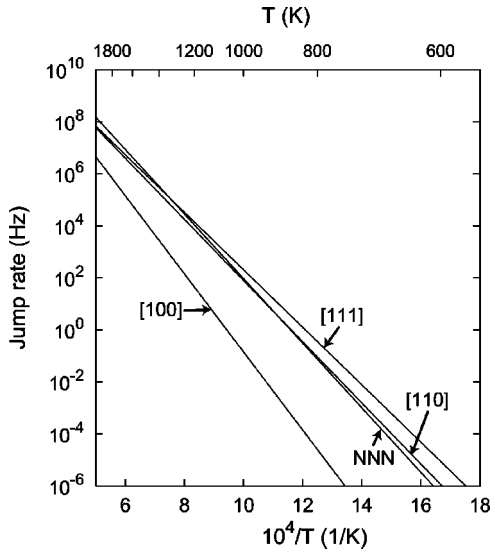

FIG. 6. Calculated temperature dependence of rate constants of collective [100], [110], and [111] jumps as well as NNN jumps of a Ni vacancy in NiAl.

The energy maxima on the reaction paths in Fig. 3 correspond to saddle-points of the jumps. The energy barriers and attempt frequencies of the jumps calculated within the transition state theory are summarized in Table IV. The jump rates calculated from Eq. (2) are plotted in Fig. 6. The plots demonstrate that collective [100] jumps have the lowest rate at all temperatures. Because such jumps initiate [100] 6JCs and since the barriers of medium jumps of such cycles are relatively high [Fig. 5], this observation suggest [100] 6JCs are unfavorable. This conclusion is in agreement with previous calculations.[6,9] The rates of NNN jumps and collective [110] jumps are very close to one another, suggesting that both the NNN vacancy and [110] 6JC mechanisms can contribute to Ni diffusion. It should be noted, however, that Fig. 6 may overestimate the relative importance of [110] 6JCs since the latter contain another jump barrier [cf. Fig. 5(a)]. In addition, the effective jump rate of the [110] 6JC mechanism can be reduced due to jump correlation effects.[8,22] Rigorous kinetic calculations similar to those of Refs. 8 and 22 would be needed for a full evaluation of the [110] 6JC mechanism. Finally, collective [111] jumps are probably the most frequent events in NiAl, especially at low temperatures (Fig. 6). It is not clear at this point if and how they can lead to long-range diffusion. Most likely, such jumps will only create short-lived configurations eliminated by a reverse jump, but we cannot exclude that they can also work as a mechanism of antisite defect generation at high temperatures.

IV. CONCLUSIONS

NiAl is a triple-defect compound in which Ni vacancies strongly dominate over Al vacancies and are likely to play a key role in atomic diffusion of both Ni and Al. Several atomic mechanisms of diffusion can operate in NiAl concurrently and may depend on the composition around the stoichiometry. In this work, we have studied the energetics of Ni vacancy jumps in the perfectly ordered stoichiometric structure of NiAl. An EAM potential fit to experimental and first-principles data has been used and the key results have been verified by additional first-principles calculations. The results can be summarized as follows:

1. The configuration arising after an NN jump of a Ni vacancy is mechanically unstable. As a result of this instability, the vacancy implements two sequential NN jumps as one collective, two-atom displacement.

2. The collective vacancy jumps by vectors [100] and [110] initiate 6JCs. Due to the symmetry of such cycles, the reversals of these jumps complete the respective 6JCs. Furthermore, for [110] 6JCs the central configuration turns out to be also mechanically unstable, with the consequence that the two medium NN jumps occur as one collective two-atom displacement. It follows that [110] 6JCs of a Ni vacancy in NiAl occur by three and not six vacancy jumps, in agreement with the earlier suggestion by Gumbsch.[21] The [100] 6JCs involve four vacancy jumps since the central configuration is stable.

3. Calculations within the transition state theory show that collective [110] jumps of a Ni vacancy have a larger rate constant than collective [100] jumps. Given also the higher barriers of the medium jumps, we conclude that [110] 6JCs of a Ni vacancy in NiAl are likely to dominate over [100] 6JCs.

4. NNN jumps of a Ni vacancy have a low enough energy barrier and high enough rate constant to be considered as a plausible mechanism of Ni diffusion that can operate concurrently with other mechanisms.

Work is now in progress to additionally verify these conclusions by molecular dynamics simulations.[46] An additional verification is essential since NEB calculations are based on a choice of the initial and final states of every atomic transition. The NEB method, therefore, can never guarantee that some unanticipated transitions are not missed in the calculations. Given this fact, we cannot claim that we have presented the complete picture of diffusion in NiAl, even though we believe that the most important mechansims have been captured. The ongoing molecular-dynamics simulations[46] have only revealed three types of Ni vacancy jumps: NNN jumps, [110] 6JCs implemented by three two-atom transitions, and two-atom [111] jumps. The latter are short-lived and reverse after less than a picosecond. Thus, no transitions other than those considered in this paper have been observed so far. It should be recognized, however, that a detailed analysis of diffusion mechanisms by molecular dynamics is a challenging problem because of the limited time scale accessible by this method. Some of the challenges can be addressed by applying new methods that recently appeared in the literature,[47] as it was done, for example, in Refs. 48 and 49. The application of those methods to diffusion in NiAl will be the subject of our future work.

It should be pointed out that the model in which Ni diffusion is mediated by Ni vacancies and does not involve any preexisting antisites may apply to both the stoichiometric and slightly Al-rich compositions of NiAl. In Ni-rich compositions, Ni_{Al} antisites may interfere with 6JCs and affect the energetics on NNN jumps. An analysis of these effects

and alternative diffusion mechanisms (especially the triple-defect one[4]) together with kinetic calculations of diffusion constants are required to explain the concentration dependence of Ni diffusivity observed experimentally.[3,4] Diffusion mechanisms of Al atoms is another topic that should be addressed in the future using the simulation methods applied in this work.

ACKNOWLEDGMENTS

This work was supported by the US Air Force Office of Scientific Research through Grant No. F49620-01-0025. The authors are grateful to S. V. Divinski for carefully reading the manuscript and making a number of useful comments and suggestions.

[1] D.B. Miracle, Acta Metall. Mater. **41**, 649 (1993).
[2] A.J. Bradley and A. Taylor, Proc. R. Soc. London, Ser. A **159**, 56 (1937).
[3] G.F. Hancock and B.R. McDonnel, Phys. Status Solidi A **4**, 143 (1971).
[4] S. Frank, S.V. Divinski, U. Södervall, and Chr. Herzig, Acta Mater. **49**, 1399 (2001).
[5] H. Hahn, G. Frohberg, and H. Wever, Phys. Status Solidi A **79**, 559 (1983).
[6] Y. Mishin and D. Farkas, Philos. Mag. A **75**, 187 (1997).
[7] E.W. Elcock and C.W. McCombie, Phys. Rev. **109**, 6 (1958).
[8] M. Arita, M. Koiwa, and S. Ishioka, Acta Metall. **37**, 1363 (1989).
[9] S. Divinski and Chr. Herzig, Intermetallics **8**, 1357 (2000).
[10] C.R. Kao and Y.A. Chang, Intermetallics **1**, 237 (1993).
[11] N.A. Stolwijk, M. van Gend, and H. Bakker, Philos. Mag. A **42**, 783 (1980).
[12] Y. Mishin and D. Farkas, Scr. Mater. **39**, 625 (1998).
[13] Y. Mishin and Chr. Herzig, Acta Mater. **48**, 589 (2000).
[14] Y. Mishin and D. Farkas, Philos. Mag. A **75**, 169 (1997).
[15] R.D. Hatcher, R. Zeller, and P.H. Dederichs, Phys. Rev. B **19**, 5083 (1979).
[16] J.R. Fernandez and A.M. Monti, Phys. Status Solidi B **179**, 337 (1993).
[17] S.B. Debiaggi, P.M. Decorte, and A.M. Monti, Phys. Status Solidi B **195**, 37 (1996).
[18] J.R. Fernandez, A.M. Monti, and R.C. Pasianot, J. Nucl. Mater. **229**, 1 (1996).
[19] J.R. Fernandez, A.M. Monti, and R.C. Pasianot, Phys. Status Solidi B **219**, 245 (2000).
[20] Y. Mishin, M.R. Sørensen, and A.F. Voter, Philos. Mag. A **81**, 2591 (2001).
[21] P. Gumbsch (private communication).
[22] R. Drautz and M. Fähnle, Acta Mater. **47**, 2437 (1999).
[23] Y. Mishin, M.J. Mehl, and D.A. Papaconstantopoulos, Phys. Rev. B **65**, 224114 (2002).
[24] M.S. Daw and M.I. Baskes, Phys. Rev. B **29**, 6443 (1984).
[25] V. Paidar, L.G. Wang, M. Šob, and V. Vitek, Modell. Simul. Mater. Sci. Eng. **7**, 369 (1999).
[26] CPMD, version 3.3, written by J. Hutter, A. Alavi, T. Deutsch, and the group of M. Parrinello at the MPI in Stuttgart and IBM research laboratory in Zurich.
[27] N. Troullier and J.L. Martins, Phys. Rev. B **43**, 1993 (1991).
[28] *Smithells Metals Reference Book*, 6th ed., edited by E.A. Brandes (Butterworths, London, 1983).
[29] J.W. Otto, J.K. Vassiliou, and G. Frommeyer, J. Mater. Res. **12**, 3106 (1997).
[30] K. Rzyman, Z. Moser, R.E. Watson, and M. Weinert, J. Phase Equilib. **19**, 106 (1998).
[31] A.Y. Lozovoi, A. Alavi, P.A. Korzhavyi, and M.W. Finnis, in *Properties of Complex Inorganic Solids*, edited by A. Meike, A. Gonis, P.E.A. Turchi, and K. Rajan (Kluwer Academic/Plenum, New York, 2000), Vol. 2, p. 439; A. Alavi, A.Y. Lozovoi, and M.W. Finnis, Phys. Rev. Lett. **83**, 979 (1999).
[32] G.H. Vineyard, J. Phys. Chem. Solids **3**, 121 (1957).
[33] G. Henkelman, G. Johannesson, and H. Jönsson, in *Theoretical Methods in Condensed Phase Chemistry*, edited by S.D. Schwartz (Kluwer Academic, Dordrecht, 2000), Vol. 5, Chap. 10.
[34] H. Jönsson, G. Mills, and K.W. Jacobsen, in *Classical and Quantum Dynamics in Condensed Phase Simulations*, edited by B.J. Berne, G. Ciccotti, and D.F. Coker (World Scientific, Singapore, 1998), p. 1.
[35] E.A. Guggenheim, *Thermodynamics. An Advanced Treatment for Chemistis and Physicists*, 4th ed. (Elsevier Science, North Holland, 1993).
[36] P.A. Korzhavyi, A.V. Ruban, A.Y. Lozovoi, Y.K. Vekilov, I.A. Abrikosov, and B. Johansson, Phys. Rev. B **61**, 6003 (2000).
[37] B. Meyer and M. Fähnle, Phys. Rev. B **59**, 6072 (1999).
[38] M. Hagen and M.W. Finnis, Philos. Mag. A **77**, 447 (1998).
[39] P. A. Korzhavyi, I.A. Abrikosov, and B. Johansson, in *Properties of Complex Inorganic Solids*, edited by A. Meike, A. Gonis, P.E. A. Turchi, and K. Rajan (Kluwer Academic/Plenum, New York, 2000), Vol. 2, p. 63.
[40] E.-T. Henig and H.L. Lukas, Z. Metallkd. **66**, 98 (1975).
[41] J. Philibert, *Atom Movements* (Les Editions de Physique, Les Ulis, 1991).
[42] M. Ludwig and P. Gumbsch, Modell. Simul. Mater. Sci. Eng. **3**, 533 (1995).
[43] R. Fletcher, *Practical Methods of Optimization* (Wiley, New York, 1980), Vol. 1.
[44] C.L. Fu, Y.Y. Ye, M.H. Yoo, and K.M. Ho, Phys. Rev. B **48**, 6712 (1993).
[45] G. Henkelman, B.P. Uberuaga, and H. Jónsson, J. Chem. Phys. **113**, 9901 (2000).
[46] Y. Mishin (unpublished).
[47] A.F. Voter, F. Montalenti, and T.C. Germann, Ann. Rep. Mater. Res. **32**, 321 (2002).
[48] G. Henkelman and H. Jónsson, J. Chem. Phys. **115**, 9657 (2001).
[49] F. Montalenti, M.R. Sørensen, and A.F. Voter, Phys. Rev. Lett. **87**, 126101 (2001).